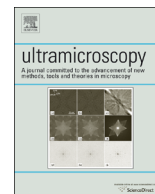




ELSEVIER

Contents lists available at SciVerse ScienceDirect

Ultramicroscopy

journal homepage: www.elsevier.com/locate/ultramic

Imaging spin filter for electrons based on specular reflection from iridium (001)



D. Kutnyakhov^a, P. Lushchik^a, A. Fognini^b, D. Perriard^b, M. Kolbe^a, K. Medjanik^a, E. Fedchenko^a, S.A. Nepijko^a, H.J. Elmers^a, G. Salvatella^b, C. Stieger^b, R. Gort^b, T. Bähler^b, T. Michlmayer^b, Y. Acremann^b, A. Vaterlaus^b, F. Giebels^c, H. Gollisch^c, R. Feder^c, C. Tusche^d, A. Krasnyuk^d, J. Kirschner^d, G. Schönhense^{a,*}

^a Johannes Gutenberg-Universität, Institut für Physik, 55099 Mainz, Germany

^b Laboratorium für Festkörperphysik, ETH Zürich, 8093 Zürich, Switzerland

^c Universität Duisburg-Essen, Theoretische Festkörperphysik, 47057 Duisburg, Germany

^d Max Planck-Institut für Mikrostrukturphysik, 06120 Halle, Germany

ARTICLE INFO

Available online 8 April 2013

Keywords:

Hemispherical electron energy analyzer

Imaging spin filter

Ir (001)

Multichannel spin detection

ABSTRACT

As Stern–Gerlach type spin filters do not work with electrons, spin analysis of electron beams is accomplished by spin-dependent scattering processes based on spin–orbit or exchange interaction. Existing polarimeters are single-channel devices characterized by an inherently low figure of merit (FoM) of typically 10^{-4} – 10^{-3} . This single-channel approach is not compatible with parallel imaging microscopes and also not with modern electron spectrometers that acquire a certain energy and angular interval simultaneously. We present a novel type of polarimeter that can transport a full image by making use of k -parallel conservation in low-energy electron diffraction. We studied specular reflection from Ir (001) because this spin-filter crystal provides a high analyzing power combined with a “lifetime” in UHV of a full day. One good working point is centered at 39 eV scattering energy with a broad maximum of 5 eV usable width. A second one at about 10 eV shows a narrower profile but much higher FoM. A relativistic layer-KKR SPLEED calculation shows good agreement with measurements.

© 2013 Elsevier B.V. All rights reserved.

1. Introduction

Stern–Gerlach-type spin filters for electrons are impossible because of the interplay between Lorentz force and Heisenberg uncertainty relation. Spin analysis of electron beams is accomplished by spin dependent scattering processes that are based on spin–orbit or exchange interaction. In the high energy range Mott-scattering at high- Z targets or Moller scattering at ferromagnetic targets are exploited. In the energy range below 100 eV spin polarized low energy electron diffraction (SPLEED) at high- Z single crystals or at ferromagnetic surfaces can be utilized (for details, see textbooks [1–3]). All of these are inherently single-channel methods. The spin-detection efficiency is given by the *figure of merit* (definition see Eq. (1)). Mostly used spin polarimeters of the present generation (Mott detector [4] or SPLEED detector [5,6] utilizing the (2,0)-reflexes from a W (001) surface) are characterized by a low figure of merit of about 10^{-4} . Two orders of magnitude can be gained via exchange scattering from an Fe surface [7–10]. Lateral resolution can only be achieved by scanning

the electron beam across a sample like in scanning electron microscopy with polarization analysis (SEMPA).

A strong discrepancy is visible when comparing spin detector development with the development of electron spectrometers. The advent of multichannel detection increased detection efficiency by orders of magnitude. A modern hemispherical analyzer acquires a certain energy and angular interval simultaneously, detecting up to 10^4 data points in parallel. Comparing a hemispherical energy analyzer with multichannel intensity detection and a spectrometer with state-of-the-art single channel spin polarimeter, we are facing a total loss in detection efficiency by 6–7 orders of magnitude!

Our basic idea for a substantial improvement of the performance of spin detectors was to *conserve the lateral distribution* of the electrons in a beam during the scattering process. In photoemission electron microscopy (PEEM) it requires to implement a reflection-type spin filter into the column of the microscope. In electron spectrometer applications, it means to adopt the multichannel detection concept that was so effective in intensity spectroscopy. The new approach exploits that an electron-diffraction process can transmit lateral image information. Owing to \vec{k}_{\parallel} momentum conservation, the specular beam in low-energy electron diffraction (LEED) behaves like a photon beam reflected at

* Corresponding author.

E-mail address: schoenhense@uni-mainz.de (G. Schönhense).

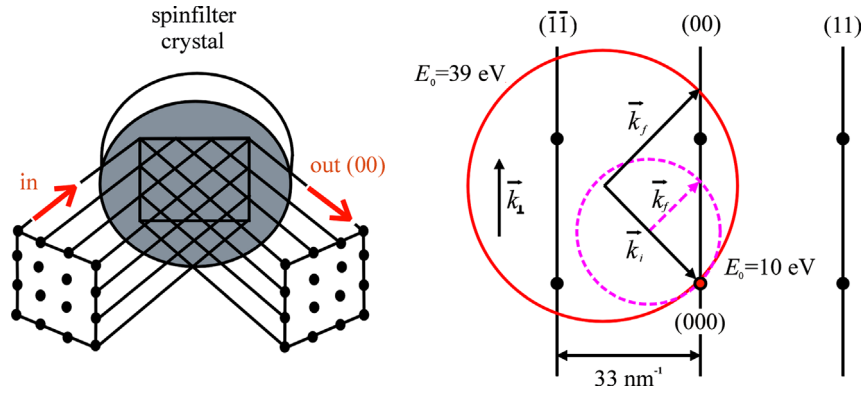


Fig. 1. Functioning scheme of the imaging spin filter in real (left) and reciprocal space (right). The size of the Ewald sphere is determined by the scattering energy, here scaled for the case of Ir (001) and 39 eV (full circle) and 10 eV scattering energy (dashed circle). k_i and k_f denote the wave vectors of incoming and outgoing beams.

an optical mirror. The idea to exploit \vec{k}_{\parallel} -conservation in a SPLEED setup brought up the concept of *2D electron spin filtering of PEEM images* [11,12]. Moreover, it opened the door to a substantial improvement of spin detection efficiency in spectroscopic applications, e.g. behind a *hemispherical electron spectrometer* [13–15] and in the future spin filtering of momentum distributions.

The functioning principle is the same for all these applications. It is illustrated in Fig. 1 for the idealized case of a perfectly parallel beam specularly diffracted at a single-crystal surface. In this case the image information is “encoded” in the lateral coordinate on the spin-filter crystal. Alternatively, a crossover could be focused on the spin filter. In that case the image information would be encoded in the scattering angle. The Ewald construction in reciprocal space (right figure) corresponds to specular reflection from Ir (001) at 45° impact angle. The full and dashed circles denote the Ewald sphere for the high- and low-energy working points (see below), i.e. 39 and 10 eV scattering energy, respectively. Note that for the latter case the Ewald sphere is so small that no other reflex besides the specular (0,0)-reflex exists.

Optimum working points are defined by the extrema in the (single-channel) figure of merit, given by

$$\text{FoM}_{\text{single}} = S^2 I / I_0, \quad (1)$$

depending on the square of the spin sensitivity S (also termed Sherman function [1]) and reflectivity I/I_0 . In addition, the number of simultaneously acquired data points must be large. The relevant statistical quantity for obtaining spin-filtered 2D images is the *two-dimensional figure of merit*

$$\text{FoM}_{2D} = N < \text{FoM}_{\text{single}} >, \quad (2)$$

where N is the number of data points taken simultaneously and $< \text{FoM}_{\text{single}} >$ is the single-channel figure of merit averaged over the utilized energy and angle interval [11,13]. We will see in the next section that reflectivity and spin asymmetry vary strongly with scattering energy and angle.

Up to now, most experiments were done using specular diffraction from W (001) under 45° angle of incidence. At a scattering energy of 27 eV the asymmetry function reaches its maximum of $S=0.42$ at a reflectivity of $I/I_0=1.3\%$, yielding $\text{FoM}_{\text{single}}=2 \times 10^{-3}$. In the imaging spin filter behind a PEEM parallel detection of $N=3800$ data points was achieved, leading to a corresponding figure of merit of $\text{FoM}_{2D}=8$ [11]. Behind a hemispherical energy analyzer about 1000 data points could be acquired simultaneously; this corresponds to a $\text{FoM}_{2D}=1.7$ [13]. These values are about four orders of magnitude higher than the $\text{FoM}_{\text{single}}$ value of the classical Mott-detector or SPLEED detector.

The advantage of the multichannel approach has recently been demonstrated in the study of highly reactive surfaces [15] and the

extension to spin-resolved photoemission in the hard X-ray range is on its way (Spin-HAXPES was demonstrated with a single-channel spin detector [16]). Due to the low cross sections in the HAXPES regime, this technique is characterized by notoriously low count rates, demanding for multichannel detection.

It is well known from early SPLEED studies that two classes of single-crystal surfaces can show high spin asymmetries in the specular beam at certain energies. For high- Z targets the spin asymmetry is induced by spin-orbit interaction during the scattering process at the heavy atoms of the crystal as demonstrated for the “classical” system W (001) [5] and several others (Au, Pd, Pt). For ferromagnets the relevant mechanism is the exchange interaction [7–10].

As the SPLEED process is highly surface sensitive, the spinfilter crystal must be frequently cleaned. For the W (001)-detectors the initial preparation consists of oxidation cycles at 1300 K followed by short high temperature flashes to desorb the oxide. During operation, short flashes are necessary in order to desorb adsorbates like CO [6]. In order to reduce the delay time due to these flashes, we searched for a high- Z material with a much higher lifetime. Due to its low reactivity, we have chosen the Ir (001) surface for the present study. This surface is much less reactive than W (001) and should allow for longer lifetimes in UHV. The purpose of this paper is to present the spin-filter performance of Ir (001) and to show some examples of its application. A SPLEED-calculation in relativistic layer-KKR code was performed serving as valuable guideline in search for optimum working points.

2. Theory

Parallel to the experiments we explored, for the Ir (001)- 1×1 surface, the “landscape” of the figure of merit as function of scattering energy E and scattering angle θ (impact angle with respect to the surface normal). According to an earlier LEED structure analysis [17] the topmost atomic layer of Ir (001)- 1×1 is relaxed inward by about 2%. For this geometry, we computed ab initio the electronic structure of the ground state of an eleven-layer thin film within density functional theory by means of the Full-potential Linearized Augmented Plane Wave (FLAPW) computer code FLEUR [18] using a local density approximation for the exchange-correlation energy. The thus obtained real one-electron potential was augmented by a complex self-energy correction to yield the quasi-particle potential appropriate for SPLEED. The imaginary part of this self-energy correction, which accounts for the influence of inelastic scattering, was chosen as $V_i(E)=0.1(E+\Phi)^{0.83}$ eV [19], where E is the kinetic energy of the diffracted electron and $\Phi=5.91$ eV the work function of the sample as obtained by our ground state calculation. The real part of the self-energy correction is essentially

two-fold: firstly, the ground state real inner potential ($V_0=15.76$ eV) is reduced with increasing kinetic energy E ; secondly, the surface potential barrier moves closer to the topmost internuclear plane. Since these two corrections are not quantitatively known a priori, but would have to be determined by comparing calculated with experimental SPLEED spectra, we firstly used the ground state inner potential. For the surface barrier, we employed a smooth form with image asymptotics [19] and performed SPLEED calculations with parameters appropriate for the ground state as well as with values yielding an inward-displaced barrier.

Using the above quasiparticle potential, SPLEED calculations were performed by means of a relativistic layer-Korringa-Kohn-Rostoker (KKR) code [3]. The resulting E - θ landscapes for the specular beam from the Ir (001)- 1×1 surface are shown in Fig. 2 (a–c). The energy E is the kinetic energy of the SPLEED electrons relative to the vacuum level of a semi-infinite Ir (001) crystal. The scattering plane was chosen to intersect the surface along the (010) direction. Since it is a mirror plane of the semi-infinite crystal, the 00 beam spin polarization vector obtained in the case of an unpolarized primary beam is perpendicular to the scattering plane and equal to the spin asymmetry vector in the case of spin-polarized primary beams, cf. [2,3]. Complete information is

therefore contained in the spin-averaged reflectivity I/I_0 and in the spin asymmetry

$$A = (I_{\uparrow} - I_{\downarrow}) / (I_{\uparrow} + I_{\downarrow}). \quad (3)$$

With I_{\uparrow} and I_{\downarrow} denoting the specular beam intensities for a completely polarized primary beam with polarization vector perpendicular (up and down) to the scattering plane.

Since the contour plots in Fig. 2(a–c) are quite self-explanatory, it may suffice to draw attention to some salient FoM features in Fig. 2(c). Below 6 eV, a ridge with FoM values up to 0.015 extends over a wide angular range, from $\theta=6^\circ$ to $\theta=65^\circ$. These values are similar to the peak values obtained in a recent SPLEED study on Au (111) [20], which was, however, restricted to energies below 20 eV and to angles below 40° . For our present spin-filter purpose, angles between 40° and 50° are more suitable. In this angular range, the FoM in Fig. 2(c) exhibits, in addition to the already mentioned ridge, two regions with quite sizeable values, one between 7 and 14 eV, the other between 30 and 40 eV. At higher energies, there is only a smaller FoM mountain around 52 eV.

3. Experimental set up

For initial preparation and characterization of *spin-integral reflectivity* the Ir (001) crystal was studied by LEED/Auger and recipes for a “blind” preparation in the spin polarimeter were tested out. In order to investigate the *reflectivity and spin asymmetry* as function of scattering energy, the novel imaging spin filter was adapted to a hemispherical electron energy analyzer [21]. As compared to our first design [13], the lens diameters have been scaled up by a factor of 1.5 to account for the larger exit field of this analyzer. For adjustment purposes a real exit slit could be used, whereas for multichannel operation the full exit field of the spectrometer was focused in a demagnified spot onto the spin filter crystal and subsequently focused onto the 2D electron detector in a magnified image using the projective optics. The Ir crystal was mounted under a fixed polar scattering angle of 45° . The azimuthal angle could be varied by means of a high-precision rotary motion feedthrough. Azimuthal angle adjustment turned out to be crucial for optimization of the scattering asymmetry. It is known from previous measurements on W (001) [2] that the azimuthal dependence of scattering asymmetry in so-called rotation diagrams can be very pronounced and can even show sign reversals (that in principle could be utilized for elimination of apparatus-related spurious asymmetries).

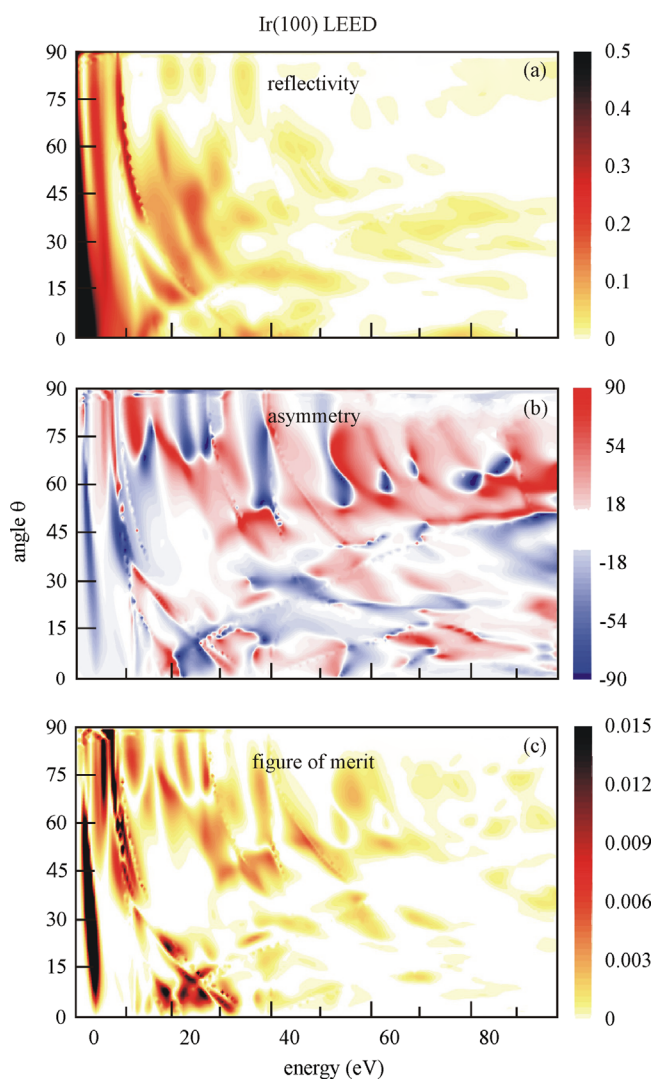


Fig. 2. E - θ landscape of reflectivity (a), spin asymmetry (b) and single-channel figure of merit (c) for unreconstructed Ir (001), calculated by the relativistic layer-KKR SPLEED code. The false color scales denote absolute spin-averaged reflectivity (a), spin asymmetry according to Eq. (3) in % (b) and absolute $\text{FoM}_{\text{single}}$ according to Eq. (1) (c). The scattering plane intersects the surface along the (010) direction.

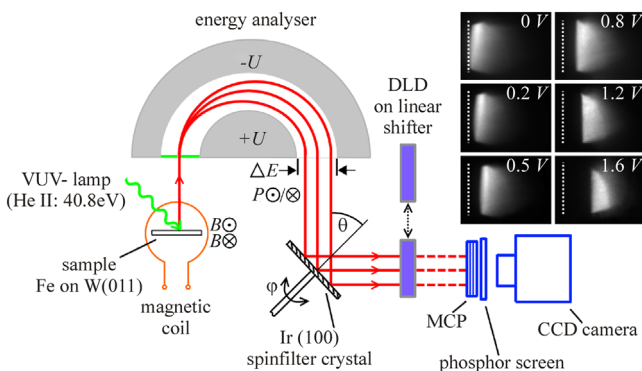


Fig. 3. Electron-optical layout of the imaging spin polarimeter in the dispersive plane (schematic: lenses omitted and scattering plane rotated by 90° with respect to the drawing plane). The spinfilter crystal is rotatable about its surface normal in order to vary the azimuthal scattering angle ϕ at fixed polar angle θ . Image series: Snapshots of the secondary-electron distribution taken behind the spinfilter crystal during an energy sweep. Note how intensity maximum and sharp low-energy cut off shift in the field of view; sweep voltages are given.

A schematic sketch of the setup is shown in Fig. 3; for sake of simplicity, all lens elements have been omitted. For all results shown below the spectrometer was operated at a pass energy of 80 eV. In this case a wide energy band can be accumulated simultaneously. The dispersion of the spectrometer at 80 eV is 0.265 eV per mm, meaning that an interval of 5.3 eV fits into an exit field of 20 mm width. In the multichannel acquisition mode the whole field of view is analyzed simultaneously. If now the kinetic energy is scanned (in the standard operation mode of the spectrometer) the whole spectrum shifts across the field of view as visible in the image series in Fig. 3. During the energy sweep, the intensities measured at a given point in the exit field are a function of the coordinate in the exit field and of the present sweep voltage. When summing up the data in the multichannel mode this relation of sweep voltage and coordinate is taken into account. A line scan across the cutoff edge in the series shown in Fig. 3 yields a resolution of 160 meV FWHM at these settings. Thus, about 33 energy points can be resolved simultaneously. In non-dispersive direction a grid could be inserted in front of the entrance lens of the spectrometer. In the low-angular-dispersion mode an interval from -7° to $+7^\circ$ polar emission angle from the sample can be accepted. From a linescan across this grid pattern we can conclude that more than 30 angular intervals can be acquired simultaneously. Hence, N in Eq. (2) is almost 1000.

The electron image could either be accumulated using the common multichannelplate – screen – CCD camera imaging unit that is normally used directly behind the electron analyzer. Alternatively we used a single-electron counting delayline detector [23], which can be moved into the beam path using a linear motion feedthrough. The delayline detector is characterized by a large dynamic range of more than 5 orders of magnitude. It has an active diameter of 40 mm, a spatial resolution of about 50 μm and a maximum count rate of 10^7 counts per second. An isolation valve of ultra-flat design (thickness of shutter plate only 2 mm) was integrated into the transfer optics between spectrometer and spin detector, in order to shut off the spin detector from the main vacuum system during preparation of the spin-filter crystal or the sample in the main chamber.

4. Experimental results

The Ir (001) crystal was prepared at a base pressure of 7×10^{-11} mbar following the guidelines of [24]. For hot oxygen treatment it was heated up to 1100–1150 K under O_2 partial pressure of 8×10^{-8} mbar during 5–10 cycles for 5 min. Subsequently a short (~ 20 s) high temperature (~ 1600 K) oxide-flash was carried out at 3×10^{-10} mbar. After this procedure the surface always showed the well-known 5×1 reconstruction [25].

Theory predicts several regions of high FoM at angles of incidence between $\theta=40^\circ$ and 50° . A scattering geometry around $\theta=45^\circ$ is very convenient for a practical design of the spin filter. Therefore, we have studied this scattering region in detail using the set-up sketched in Fig. 3. As polarized source we used the secondary electrons from an epitaxial Fe film on W (011), providing a spin polarization of 30% in the intense peak of the secondary-electron cascade [22,26].

The experimental data have been taken for freshly-deposited Fe films magnetized by an in-vacuum coil along the two directions perpendicular to the scattering plane. At each energy the spin asymmetry A was determined according to Eq. (3) from the intensity distributions I_\uparrow and I_\downarrow for opposite magnetization directions. The denominator of Eq. (3) is proportional to the spin-integral intensity. The results are summarized in Fig. 4(a–i) together with line scans in the theoretical E – θ landscape along $\theta=45^\circ$. In addition, sections of the false-color plots of reflectivity,

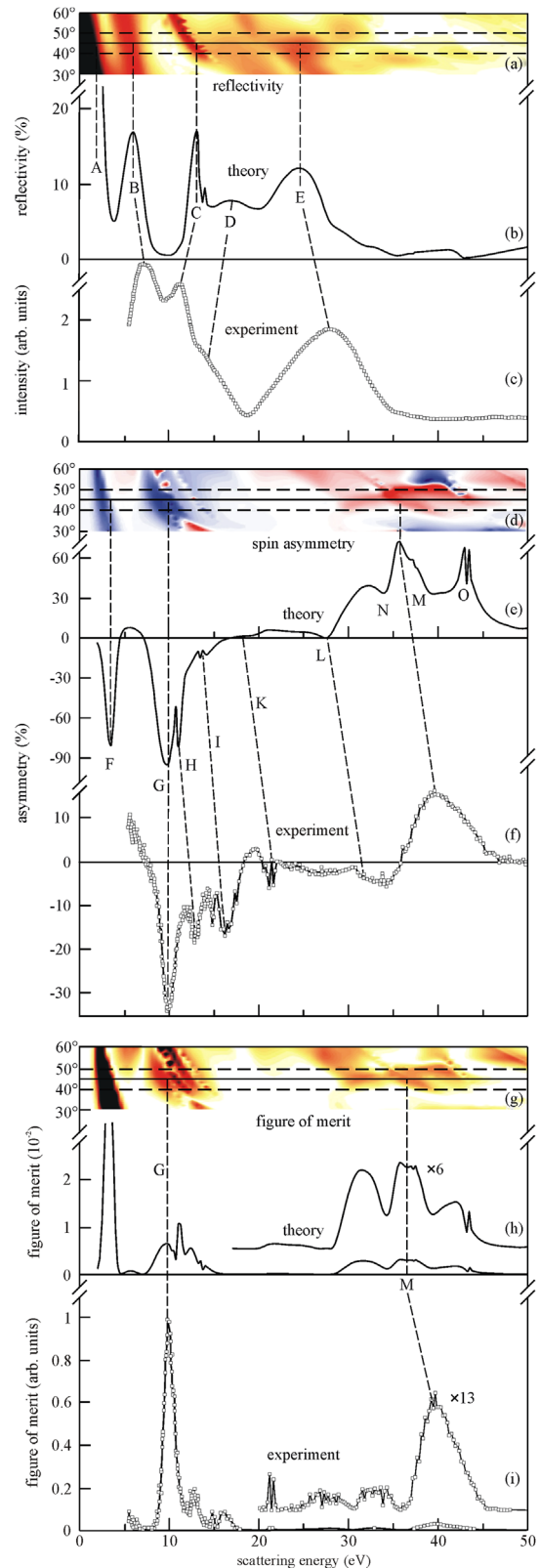


Fig. 4. Results for reflectivity (a–c), spin asymmetry (d–f) and figure of merit (g–i) for elastic specular scattering from Ir (001) at $\theta=45^\circ$. Note that the measurement was taken for the 5×1 reconstructed surface (c, f, i), whereas the calculations assumed a non-reconstructed surface (b, e, h). The false-color plots represent details of Fig. 2 in the angular range of 30° – 60° .

asymmetry and FoM between 30° and 60° are included on the same energy scale in order to illustrate the angular dependence around 45° .

The figure reveals rather good overall agreement between theory and experiment, despite the fact that the calculation and measurement were made for the unreconstructed and 5×1 reconstructed surface, respectively. Many details (G–M) of the pronounced structure of the measured spin asymmetry (spectrum f) agree well with theory (spectrum e). For the reflectivity the agreement is obviously worse, both concerning signal positions (e.g. B and C) and intensity (e.g. deep minimum in experimental spectrum (c) between signals D and E). The measured figure of merit (spectrum i) reveals two prominent working points in this energy range below 50 eV, as predicted by theory (spectrum h). Again, significant deviations are obvious. In the following, we will discuss these results in detail.

The experimental and theoretical energy scales have been adjusted at the pronounced negative peak G in the asymmetry curve at low energies. Best agreement was achieved by a small shift of the experimental curve (by 1 eV) to higher energy. The energy scale of the experiment is derived from the potential difference (including the workfunction difference) between the electron source (in this case the secondary electron signal of the iron film with the kinetic energy being selected by the spectrometer) and the spin filter crystal. The theoretical energy scale from Figs. 2(a–c) and 4(a–i) is the kinetic energy of the diffracted electrons with respect to the vacuum level above a semi-infinite iridium crystal. The diffraction energy inside of the material depends on the quasi-particle inner potential, which is not known quantitatively. For the results shown in Fig. 2(a–c) we had taken the ground state inner potential $V_0=15.76$ eV. In a future experiment we will determine the true scattering energy using a time-of-flight technique and thence also the quasi-particle inner potential.

The *low energy working point* at about 10 eV scattering energy is characterized by a high peak in the figure of merit (theoretical value 1×10^{-2}) but relatively narrow usable energy band of about 1 eV FWHM. This is a favorable working point for high-resolution applications. The measured spectral variation of the spin asymmetry (f) agrees in many details with the theory curve (e). The asymmetry values of the experiment are consistently smaller, similar as found for the Au(111) case [20]. For the shown measurement sequence an experimental asymmetry maximum of 11% at the given primary polarization of 30% [22,26] we derive a maximum asymmetry function S of 37% in peak G. This value is about a factor of two smaller than the theoretical prediction. In later measurements after many more preparation cycles the asymmetry extremum value increased to about 70%, still somewhat smaller than the theoretical value of 95%. We conclude that there are contributions to the scattering process that are not included or not treated properly in the theoretical code. An intrinsic contribution may be incoherent (elastic) scattering, an indication being that the intensity minima in Figs. 4 and 5(c) are not as deep as their theoretical counterparts. As possible extrinsic reasons we can name the limited energy and angular resolution of the electron beam at the spin filter crystal. The theoretical profile shows wings at both sides of the sharp maximum, the measurement (spectrum i) reveals a wing only on the high-energy side.

The dashed lines and labels G–M denote characteristic features that agree quite well. Polarization feature F is not visible in experiment, most likely due to strong quenching of such low kinetic energies as 5 eV by spurious magnetic fields. Theoretical features N and O are also not visible. Possibly they are smeared out and merge into the broad experimental peak M.

The sections of the $E-\theta$ landscape indicate the angular variation of the features. We see that the negative asymmetry extremum G is centered at about $\theta=45^\circ$, see dark blue feature in (d). Above 52° and below 35° it is accompanied by regions of reverse asymmetry as visible in the red regions in (d). We will see below that these in fact occur in the scattering patterns.

The *high-energy working point* is characterized by a broad maximum of positive asymmetry M centered at about 39 eV. The FoM curve shows a FWHM of 5 eV, meaning that this working point is well suited for cases where a large energy band is analyzed simultaneously.

It lies on the high-energy side of the intensity feature E. Experimentally, the intensity feature is broadened and does not show a splitting into several maxima as predicted by theory. The theoretical maximum N is merged into the broad peak M and the sharp double peak O is missing in the measured asymmetry curve. In the asymmetry landscape (d) the maximum shows up at significantly larger angles of incidence of almost 50° (dark red feature in d). This is different from the low-energy point, where both extrema intersect the 45° line. An interesting feature is visible around 33 eV scattering energy, i.e. in the wing of the intensity maximum. We observe a clear negative asymmetry feature L (in theory only a small dip reaching zero asymmetry). This negative extremum offers the possibility of *asymmetry reversal* for zero calibration by taking electron distributions in the 39 and 33 eV extrema.

In search for the origin of the discrepancies between experiment and theory we found that they cannot be removed by physically reasonable changes of the input parameters to our SPLEED calculations for the unreconstructed surface, in particular not by displacements of the surface potential barrier. This leaves us with ascribing them to genuine differences of the SPLEED spectra for the 1×1 and the 5×1 surface geometry.

It is clear from Fig. 3 that the scattering energy varies along the lateral coordinate in the drawing plane, also called *dispersive plane* because electrons with different energies are dispersed in this plane. In the *non-dispersive plane* perpendicular to the drawing plane different angles are “sorted”, up to an interval of $\pm 15^\circ$ emission angle from the sample. The electron optics can be adjusted in such a way that the variation of the emission angle at the sample shows up in terms of a variation of the scattering angle at the spin filter crystal. Under such conditions, the lateral coordinates in the observed pattern correspond to scattering energy and angle and one can directly observe a small section of the 2D landscape like the inset (d) in Fig. 4. Such measurements are performed in a spectral region where the spin polarization of the source signal is constant. An example of this kind of measurement is shown in Fig. 5. A comparison of theory (panel a) and experiment (panel b) reveals in both cases a characteristic bipolar asymmetry feature in the low-energy region between 10 and 15 eV scattering energy and 30° and 50° scattering angle. The asymmetry maximum of 20% corresponds to a spin sensitivity (Sherman function) of about 70%. The wavy structure in the image results from a grid that can be shifted into the electron optical path for optimizing the angular resolution in test experiments. For real spectroscopic measurements the grid is retracted. Systematic measurements of this kind will allow mapping out the full 2D asymmetry landscape. For normal measurements the electron optics is adjusted such that the asymmetry function varies only little across the field of view. Such a case is shown in Fig. 5(c). In this working point the asymmetry is practically homogeneous and the vertical scale directly represents the emission angle from the sample, as denoted by the right ordinate. Here, the angular grid was retracted. In general, the variation of the asymmetry function across the field of view must be taken into account via the image acquisition software (see also paper by Tusche et al., this issue [12]).

Typical spectra taken with this set up are shown in Fig. 6. The left panel (a) shows a spin-resolved spectrum of the secondary electrons, after excitation with 10 keV electrons. The spectrum agrees fairly well with literature data. The feature above 12 eV was also observed in previous work [22,26] and is presumably a final-state feature. The right panel (b) shows a spin-resolved photoelectron spectrum taken with a Helium lamp. The spectrum shows

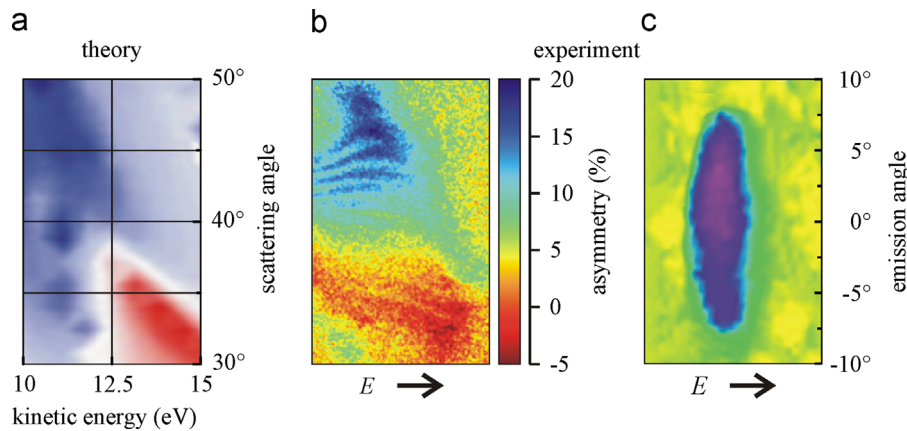


Fig. 5. Theoretical asymmetry pattern around the low-energy working point. Detail of Fig. 2(b) is given in (a). Asymmetry pattern observed in the exit plane of the analyzer in this energy vs. scattering angle region (b). The wavy structure originates from a grid inserted into the electron optical path to mark the angles. Pattern obtained at a different setting with homogeneous asymmetry function in the oval field of view (c).

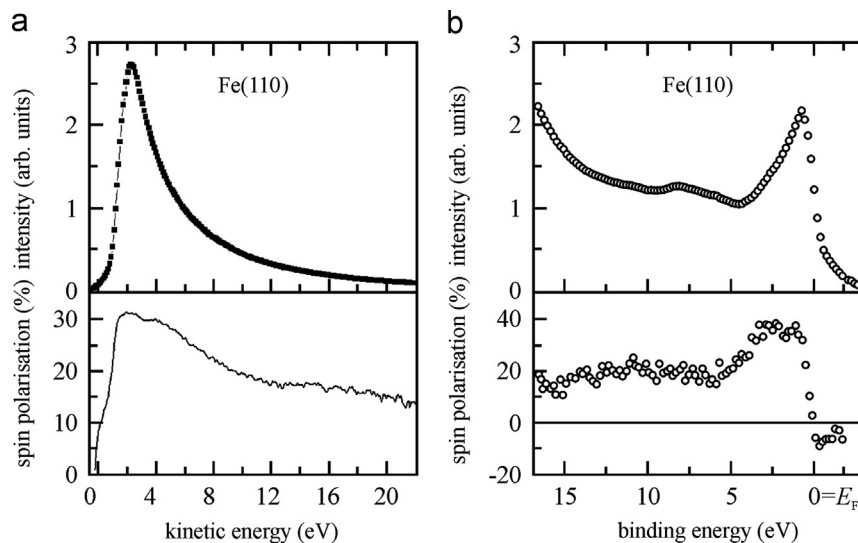


Fig. 6. Intensity and spin polarization spectra of the secondary electrons from an Fe(110) thin film induced by electron bombardment (a) and spin-resolved ARUPS spectrum of the same sample taken with He radiation (b).

the characteristic rapid drop of the spin polarization from positive values below the Fermi energy to negative values at the Fermi energy. These spectra have been taken in multichannel mode at a pass energy of 80 eV, with the exit field of the analyzer fully open, as explained in Fig. 3. For the spectrum in Fig. 6b the angular range was $\pm 7^\circ$ at an angular resolution of 0.5° . The energy resolution was about 400 meV and the spectrum was acquired in 0.5 h. Both spectra are displayed after integration over the angular coordinate. More details of the multichannel acquisition mode can be found in [13].

5. Summary and conclusion

Since the pioneering work of Kirschner and Feder in 1979 spin detectors based on spin polarized low-energy electron diffraction (SPLEED) are widely used as polarimeters in spectroscopy, for generation of magnetic images in SEMPA and, more recently, for parallel-imaging spin filters. The prototype high-Z material for SPLEED detectors is still W (001) since it is best understood and its preparation is comparably easy. The present paper is the result of the quest to find a novel material with much larger lifetime in UHV, thus avoiding the frequent flashes required for tungsten. We

found that the Ir (001) surface is a very good alternative to W (001). Its spin analyzing power is very high, the Sherman function reaches values up to 70%, it shows very good imaging properties in the spin filter application and typical lifetimes of the freshly prepared surface were about one day. As a guideline for the search for extrema in the figure of merit we calculated the reflectivity and spin asymmetry in the 2D E - θ landscape (scattering energy vs. angle of incidence) using a relativistic layer-KKR SPLEED code.

Ir (001) was first studied using LEED/Auger with emphasis placed on a reproducible preparation of the surface, being mandatory for the application as imaging spin filter. We found that the clean 5×1 reconstructed surface could be prepared reliably, whereas recipes removing the reconstruction often left residues of reconstructed regions on the surface. Thus, all measurements have been performed for the clean, reconstructed surface. First results for ultrathin layers of Au on Ir (001) suggest that this system exhibits a non-reconstructed surface and offers the chance for a further substantial improvement of the lifetime of the surface in UHV.

Central result is the survey study of spin asymmetry and reflectivity for the 5×1 surface in the energy region up to 50 eV at an angle of incidence of 45° in specular geometry. Two attractive working points were found in this region: At 10 eV we

find the total maximum in figure of merit in a rather narrow peak of about 1 eV width; at 39 eV scattering energy we observed a broad maximum characterized by a usable energy interval of 5 eV.

Despite of the fact that the experiment was performed for the 5×1 reconstructed surface, and theory studied the non-reconstructed surface, the overall agreement of experimental and theoretical spin asymmetry curves is rather good. We can conclude that relativistic layer-KKR SPLEED calculations provide a valuable guideline in the search for other high- Z spin filters. Generally, the agreement is significantly better for the asymmetry than for the reflectivity. In the asymmetry (Eq. (3)) many secondary influences like transport losses etc. cancel out, because they act in the same way on I_{\uparrow} and I_{\downarrow} . However, such effects alter the reflectivity.

The agreement between theory and experiment is apparently better in the low energy region. This may be due to the larger probing depth owing to the increasing inelastic mean free path at low energies. Thus, the relative contribution from the reconstructed surface is smaller in relation to the contribution from deeper-lying layers. In search for the origin of the discrepancies we found that they cannot be removed by physically reasonable changes of the input parameters to our SPLEED calculations for the unreconstructed surface, in particular not by displacements of the surface potential barrier. This leaves us with ascribing them to genuine differences of the SPLEED spectra for the 1×1 and the 5×1 surface geometry.

The results confirm that an angle of incidence of 45° is a good choice in the total E - θ landscape. The other regions with large FoM (at 6° and 18–28 eV or the low energy region above 70°) are attractive as well, but geometrically less favorable for the present experiment.

The limits of the imaging spin filter with respect to aberrations are very different for different applications. Behind the exit of a *hemispherical analyzer* we encounter a very large field of view (width 20 mm or more) and also a large angular divergence of about 4° (characteristic for hemispherical analyzers). Furthermore, the kinetic energy varies by 5–10% of the pass energy across the field of view. This leads to electron-optical aberrations that set a limit to the number of simultaneously resolvable data points. Simulations reveal that more than 40 energy intervals and 40 angular intervals (i.e. > 1600 data points) can be resolved in this mode. This value is dictated by electron-optical aberrations. Experiments to explore the limit are under way. In a *photoemission microscope* (or *momentum microscope*) the field of view is small and beam divergence can be reduced to 0.5 – 1° at the position of the spin filter. Tusche et al. [11,12] demonstrated that 4000 data points can be resolved in spin-filtered PEEM using a W (001) crystal. Unlike the first case, here the limit is set by the diffraction process, in particular the angular spread of the diffracted beam and the mosaic pattern of the spinfilter crystal. A thorough discussion of these influences and the procedure for quantitative measurements in the microscopy application is given in [12]. In a third application the imaging spin filter is combined with *time-of-flight photoelectron spectromicroscopy*. In this case, the chromatic aberration due to the energy spectrum acquired simultaneously and the width of the usable asymmetry features of the spinfilter crystal set additional requirements. For this application the 5 eV wide asymmetry profile at the high energy working point (cf. Fig. 4f) is advantageous.

The superior performance of multichannel spin detection provides a novel method for magnetic domain imaging with an efficiency higher than exploiting MCD [11]. The parallel image acquisition further paves the way to single-shot experiments at ultra-bright fs-sources like FELs. Combined with a hemispherical electron spectrometer, the spin filter improves spin detection efficiency by orders of magnitude and thus facilitates experiments on highly reactive surfaces like in-situ prepared Heusler films, radiation-sensitive organic layers or in low-intensity spectroscopy like Spin-HAXPES.

Acknowledgments

We thank Andreas Oelsner (Surface Concept GmbH) for fruitful cooperation concerning the delayline detector. The project is funded by DFG (Scho 341/9), Stiftung Rheinland Pfalz für Innovation (Projects 886 and 1038) and center for complex materials COMATT.

References

- [1] J. Kessler, Polarized Electrons, Springer, Berlin, 1976.
- [2] J. Kirschner, Polarized electrons at surfaces, vol. 106, Springer Tracts in Modern Physics, Springer; Berlin, 1985.
- [3] R. Feder, Polarized Electrons in Surface Physics, World Scientific, Singapore, 1985.
- [4] T.J. Gay, Advances in atomic, Molecular and Optical Physics 57 (2009) 157.
- [5] J. Kirschner, R. Feder, Physical Review Letters 42 (1979) 1008.
- [6] D. Yu, C. Math, M. Meier, M. Escher, G. Rangelov, M. Donath, Surface Science 601 (2007) 5803.
- [7] F.U. Hillebrecht, R.M. Jungblut, L. Wiebusch, C. Roth, H.B. Rose, D. Knabben, C. Bethke, N.B. Weber, S. Manderla, U. Rosowski, E. Kisker, Review of Scientific Instruments 73 (2002) 1229.
- [8] R. Bertacco, M. Merano, F. Ciccacci, Applied Physics Letters 72 (1998) 2050.
- [9] A. Winkelmann, D. Hartung, H. Engelhard, C.T. Chiang, J. Kirschner, Review of Scientific Instruments 79 (2008) 083303.
- [10] T. Okuda, Y. Takeichi, Y. Maeda, A. Harasawa, I. Matsuda, T. Kinoshita, A. Kakizaki, Review of Scientific Instruments 79 (2008) 123117.
- [11] C. Tusche, M. Ellguth, A.A. Unal, C.T. Chiang, A. Winkelmann, A. Krasnyuk, M. Hahn, G. Schönhense, J. Kirschner, Applied Physics Letters 99 (2011) 032505.
- [12] C. Tusche, M. Ellguth, A. Krasnyuk, A. Winkelmann, D. Kutnyakhov, P. Lushchik, K. Medjanik, G. Schönhense, J. Kirschner, Ultramicroscopy, <http://dx.doi.org/10.1016/j.ultramicro.2013.02.022>, this issue.
- [13] M. Kolbe, P. Lushchik, B. Petereit, H.J. Elmers, G. Schönhense, A. Oelsner, C. Tusche, J. Kirschner, Physical Review Letters 107 (2011) 207601.
- [14] M. Hahn, G. Schönhense, E.A. Jorge, M. Jourdan, Applied Physics Letters 98 (2011) 232503.
- [15] M. Kolbe, S. Chadov, E.A. Jorge, G. Schönhense, C. Felser, H.J. Elmers, M. Kläui, M. Jourdan, Physical Review B 86 (2012) 024422.
- [16] G. Stryganyuk, X. Kozina, G.H. Fecher, S. Ouardi, S. Chadov, C. Felser, G. Schönhense, P. Lushchik, A. Oelsner, P. Bernhard, E. Ikenaga, T. Sugiyama, H. Sukegawa, Z. Wen, K. Inomata, K. Kobayashi, Japanese Journal of Applied Physics 51 (2012) 016602.
- [17] G. Besold, K. Heinz, E. Lang, K. Müller, Journal of Vacuum Science and Technology A 1 (1983) 1473.
- [18] (www.flapw.de).
- [19] S.N. Samarin, J.F. Williams, A.D. Sergeant, O.M. Artamonov, H. Gollisch, R. Feder, Physical Review B 76 (2007) 125402.
- [20] S.N. Samarin, J.F. Williams, O.M. Artamonov, J. Henk, R. Feder, Surface Science 604 (2010) 1833.
- [21] SPECS Phoibos 150.
- [22] R. Allenspach, M. Landolt, Surface Science Letters 171 (1986) L479.
- [23] A. Oelsner, O. Schmidt, M. Schicketan, M. Klais, G. Schönhense, V. Mergel, O. Jagutzki, H. Schmidt-Böcking, Review of Scientific Instruments 72 (2001) 3968.
- [24] R.G. Musket, W. McLean, C.A. Colmenares, D.M. Makowiecki, W.J. Siekhaus, Applications of Surface Science 10 (1982) 143.
- [25] S. Lehwald, J.G. Chen, G. Kisters, E. Preuss, H. Ibach, Physical Review B 43 (1991) 3920.
- [26] M. Landolt, Applied Physics A 41 (1986) 83.